Synthesis and Photocatalytic Activity of $Zn_xCd_{1-x}S/TiO_2$ Heterostructures Nanofibre Prepared by Combining Electrospinning and Hydrothermal Method

Wei Chang[a,b,*], Xiaosai Ren[a], Guorui Yang[b], Wei Yan[b,*] and Yanrong Guo[a]

[a]*School of Environmental and Chemical Engineering, Xi'an Polytechnic University, Xi'an 710048, China.*
[b]*Department of Environmental Science & Engineering, Xi'an Jiaotong University, Xi'an 710049, China.*

Received 22 October 2014, revised 30 April 2014, accepted 11 May 2015.

ABSTRACT

The $Zn_xCd_{1-x}S/TiO_2$ hierarchical heterostructures were successfully fabricated by combining electrospinning technology and hydrothermal methods. The morphology, crystallinity, composition and band gap of $Zn_xCd_{1-x}S/TiO_2$ were characterized by SEM, XRD, EDS, and UV-vis diffuse reflectance spectroscopy. The results indicated the sulphur concentration had a significant influence on the composition and morphology of the products. The values of the band gap energy for $Zn_xCd_{1-x}S/TiO_2$ varied from 2.33 to 2.66 eV with the change of sulphur concentration. When the molar ratio of S/Ti was 0.96, the $Zn_xCd_{1-x}S/TiO_2$ hierarchical heterostructures exhibited enhanced visible light photocatalytic behaviour for the decomposition of Rhodamine B (RhB) under visible light irradiation. The photocatalytic degradation of RhB followed first-order reaction kinetics.

KEYWORDS

Electrospinning, heterostructures, photocatalysis, dye degradition.

1. Introduction

The wastewater generated by the textile dying and paper-printing industries are rated as one of the most polluting among all industrial sectors. Traditional techniques can generally be used efficiently for the removal of dyes. Nevertheless, they are non-destructive since they just transfer organic compounds from water to a solid phase, which can cause secondary pollution. Photocatalytic degradation of organic contaminants has received more attention due to its high efficiency, nonselective degradation and low cost. TiO_2, which is one of the most widely studied metal oxides, has attracted significant attention in the application of the degradation of organic contaminants.[1,2] However, the relatively wide band gap (Eg = 3.0–3.2 eV) restricts the TiO_2 photo-response, which only falls into the ultraviolet region, and this only takes up 5 % of the total solar spectrum reaching the earth's surface. In order to improve the solar energy utilization of TiO_2, all kinds of modification methods have been reported, such as (1) metal ions and nonmetallic elements doping with Fe^{3+},W^{6+}, S, or N;[3–6], (2) photosensitization with organic dyes or mixed dyes such as N3[7], or N719;[8] (3) use of semiconductor composites such as CdS,[9] SnO,[10] PbS[11]. Recently, many researchers have focused on the photocatalytic property of $Zn_xCd_{1-x}S$ semiconductor composite.[12–15] By adjusting the components ratio (x value), the band gap of $Zn_xCd_{1-x}S$ can be changed. The change renders $Zn_xCd_{1-x}S$ to exhibit both high visible light photocatalytic behaviour and adjustable conduction band (CB) potential.

Electrospinning is a widely used technique, which utilizes electrical forces to produce continuous fibres with diameters down to a few nanometres. With smaller pores, higher surface area and stronger adsorption properties than regular fibres, electrospun fibres have been successfully applied in various fields, such as nanocatalysis, protective clothing and filtration[16,17] In the field of photocatalysis, the nanofibres cannot only overcome the drawback of inconvenient recycling, but also keep the higher specific surface area than film-type photocatalysts. Meanwhile, nanofibres with complex architecture can be produced by combing electrospinning and other methods.[18] Therefore, loading $Zn_xCd_{1-x}S$ on TiO_2 nanofibres will produce heterostructured nanofibres, and thus the photo-generated electron is supposed to gain greater migration power with the increase of the CB potential. As a consequence, the recombination of photogenerated electron (e^-)/hole (h^+) pairs can be greatly suppressed, and the photocatalytic activity will be enhanced.

In the present work, a novel $Zn_xCd_{1-x}S/TiO_2$ hierarchical heterostructure was fabricated by combining the electrospinning technology and hydrothermal method. The effect of sulphur concentration on the characteristic and photocatalytic activity of $Zn_xCd_{1-x}S/TiO_2$ were also investigated. Rhodamine B, an important representative dye, was used as a probe contaminant to evaluate the activity of $Zn_xCd_{1-x}S/TiO_2$ photocatalyst under visible light irradiation.

2. Materials and Methods

2.1. Chemicals and Materials

Poly(vinyl pyrrolidone) (PVP Mw ≈1.3×10^6) was obtained from BASF chemical company in Germany. Zinc acetate ($Zn(CH_3COO)_2{\cdot}2H_2O$), cadmium acetate ($Cd(CH_3COO)_2{\cdot}2H_2O$), tetrabutyl titanate ($Ti(OC_4H_9)_4$), acetic acid ($CH_3COOH$), thioacetamide (TAA) and methyl alcohol (CH_3OH) were purchased from Sinopharm Chemical Reagent Co., Ltd. Millipore water (R > 18 M Ω cm) was used in all experiments. All reagents were used as received.

2.2. Preparation of $Cd_{1-x}Zn_xS/TiO_2$ Heterostructures

2.2.1. *TiO_2 Nanofibres*

Firstly, TiO_2 precursor solution was prepared by dissolving

* To whom correspondence should be addressed. E-mail: changwei72@163.com

ISSN 0379-4350 Online / ©2015 South African Chemical Institute / http://saci.co.za/journal
DOI: http://dx.doi.org/10.17159/0379-4350/2015/v68a20

2.125 g of $Ti(OC_4H_9)_4$ in an acetic acid solution of methyl alcohol (37:3 mass ratio) coupled with vigorous stirring for 30 min. Then 1.5 g PVP powder was added to the precursor solution, and the mixture was continuously stirred for another 5 h to make a homogeneous precursor solution. 5 mL of the precursor solution was loaded into a 20 mL syringe with a stainless steel needle which was connected to a high-voltage supply (BGG Bmei Co., Ltd.). A sheet of aluminium foil was used as the collector. The distance between the needle tip and the collector was fixed at 12 cm, and the voltage was set at 12 kV. The solution was pumped continuously using a syringe pump (LSP01-1A, Baoding Longer Precision Pump Co., Ltd.) at a rate of 1.0 mL h^{-1}. The obtained composite nanofibres were calcined at 500 °C for 3 h to induce the formation of crystallized TiO_2 nanofibres.

2.2.2. *$Zn_xCd_{1-x}S/TiO_2$ Heterostructures*

Typically, 0.5 mmol $Cd(CH_3COO)_2{\cdot}2H_2O$, 0.75 mmol $Zn(CH_3COO)_2{\cdot}2H_2O$ and calculated amount of TAA (which was varied according to the molar ratio with TiO_2 as 0.5, 1, 2, 3, 4) were dissolved in 50 mL of deionized water, followed by stirring for 5 min, then 0.1 g TiO_2 nanofibres were added into the homogeneous solution. The resulting mixture was transferred into a 100 mL teflon-lined stainless steel autoclave. Then the autoclave was kept at 200 °C for 24 h. The autoclave was cooled down to room temperature after the reaction, and the obtained composite samples were washed thoroughly with deionized water and ethanol for several times, and then finally dried in a vacuum oven at 100 °C for 12 h. The obtained samples were denoted as S0.5, S1, S2, S3, S4, respectively.

2.3. Characterization

The morphology of all the samples was observed by SEM performed on a JEOL JSM 6700F field emission instrument (Japan Electronics Co. Ltd) operated at an accelerating voltage of 5.0 kV. EDS was performed on a JEOL JSM 6460 scanning electron microscope(Japan Electronics Co., Ltd). XRD patterns of the samples were collected on X'pert MPD Pro (PANalytical Co. Ltd) diffractometer using Cu Ka radiation (40 kV, 40 mA). UV-vis diffused spectroscopy of the samples were recorded using a UV4100 spectrometer (Hitachi) operating between 800 nm to 240 nm wavelength, using $BaSO_4$ as a reference.

2.4. Photocatalytic Tests

Photocatalytic performance of the samples were studied by degrading RhB simulated wastewater under visible light ($\lambda >$ 420 nm) irradiation. The photocatalytic experiments were conducted in a homemade Pyrex photochemical reactor with a quartz jacket and cooled off by circulating water. In the experiment, a 500 W xenon lamp with a cut-off filter ($\lambda > 420$ nm) was employed as the visible light source; the distance between the xenon lamp and the front surface of the reactor was fixed at 8 cm. Prior to illumination, 50 mL of RhB aqueous solutions (10 mg L^{-1}) containing 0.05 g sample were magnetically stirred in the dark for 30 min to achieve adsorption/desorption equilibrium and a good dispersion. During irradiation, about 3.0 mL of the reaction solution was withdrawn from the reactor at an interval of 10 min and centrifuged to separate the photocatalyst. The supernatant solution was analyzed by an Agilent 8430 UV-visible spectrophotometer at 554 nm, which is the maximum absorption wavelength of RhB. The remaining RhB concentration (%) after various intervals of time could be estimated using the following equation:

$$\%\ \text{RhB concentration} = C/C_0 \times 100\ \%$$

where C_0 is initial concentrations of RhB aqueous solution (that is, after the dark adsorption equilibrium), while C is the concentration at different intervals of time.

3. Results and Discussion

3.1. X-Ray Diffraction (XRD) Patterns

The XRD pattern for the as-prepared samples is shown in Fig. 1. The diffraction peaks at about 25.5 °, 37.9 °, 48.2 °, 54.1 °, 55.0 °, 62.7 °, 75.1 ° were perfectly indexed to the (101), (004), (200), (105), (211), (204), (215) crystal faces of anatase TiO_2 (JCPDS 21-1272), respectively, and diffraction peaks at about 27.5 °, 36.2 °, 41.4 °, 54.4 °, 69.0 ° were perfectly indexed to the (110), (101), (111), (211), (301) crystal faces of rutile TiO_2 (JCPDS 21-1276),[16] respectively. The mixed crystal phase of TiO_2 results in an improved photocatalytic activity. The other diffraction peaks of S0.5, S1, S2, S3, S4 were in good agreement with the $Zn_xCd_{1-x}S$, showing that the $Zn_xCd_{1-x}S/TiO_2$ composite samples were successfully synthesized. The diffraction peak of 26.8 ° appears in the spectra of sample S0.5 but disappears in the spectra of S1, S2, S3 and S4. It is speculated that the $Zn_xCd_{1-x}S$ diffraction peak of 26.8 ° has changed and overlapped with the rutile diffraction peak of 27.4 °. It was observed that peak height of rutile TiO_2 at 27.4 ° was significantly enhanced.

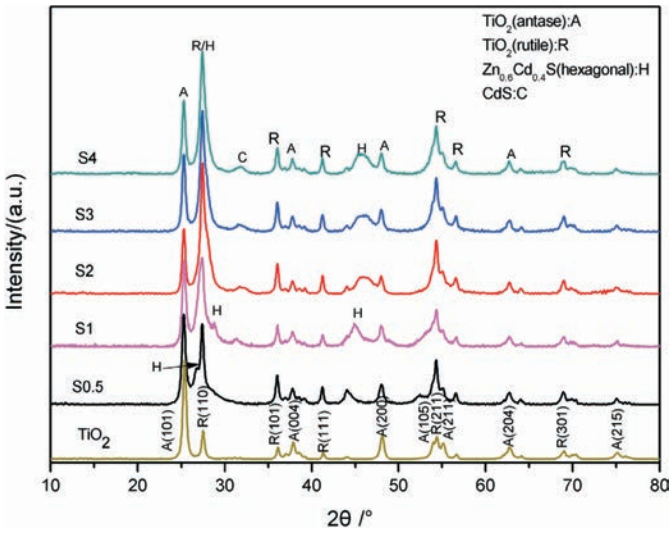

Figure 1 XRD patterns of pure TiO_2, S0.5, S1, S2, S3, S4.

3.2 SEM and EDS of the As-prepared Hierarchical Nanofibre

Figure 2a shows an SEM image of the pure TiO_2 nanofibres, which were fabricated by electrospinning followed by calcination at 500 °C for 3 h. It was clearly seen that the TiO_2 nanofibres have a relatively smooth surface and uniform thickness without secondary structures. The average fibre diameter is about 120 nm. However, as observed in of Fig. 2b–f, the $Zn_xCd_{1-x}S$ nanostructures grew on the surface of TiO_2 nanofibres after solvothermal reaction at 200 °C for 24 h. That makes the fibre diameter larger and the average fibre diameter was about 280 nm. $Zn_xCd_{1-x}S$ nanoparticles grew on the surface of TiO_2 with uniform size and uniform distribution in S0.5 and S1 (Fig. 2b–c). With the increase of the TAA concentration, the size of the $Zn_xCd_{1-x}S$ nanoparticles became different. From Fig. 2f, it was observed that the $Zn_xCd_{1-x}S$ nanoparticles became smaller, and grew on the TiO_2 nanofibres sparsely. This may be due to the fact that excessive concentration of TAA made it release too much S^{2-}. Thus S^{2-} will react with Zn^{2+} and Cd^{2+} in solution firstly to form $Zn_xCd_{1-x}S$ nanoparticles, so that the concentration of Zn^{2+} and

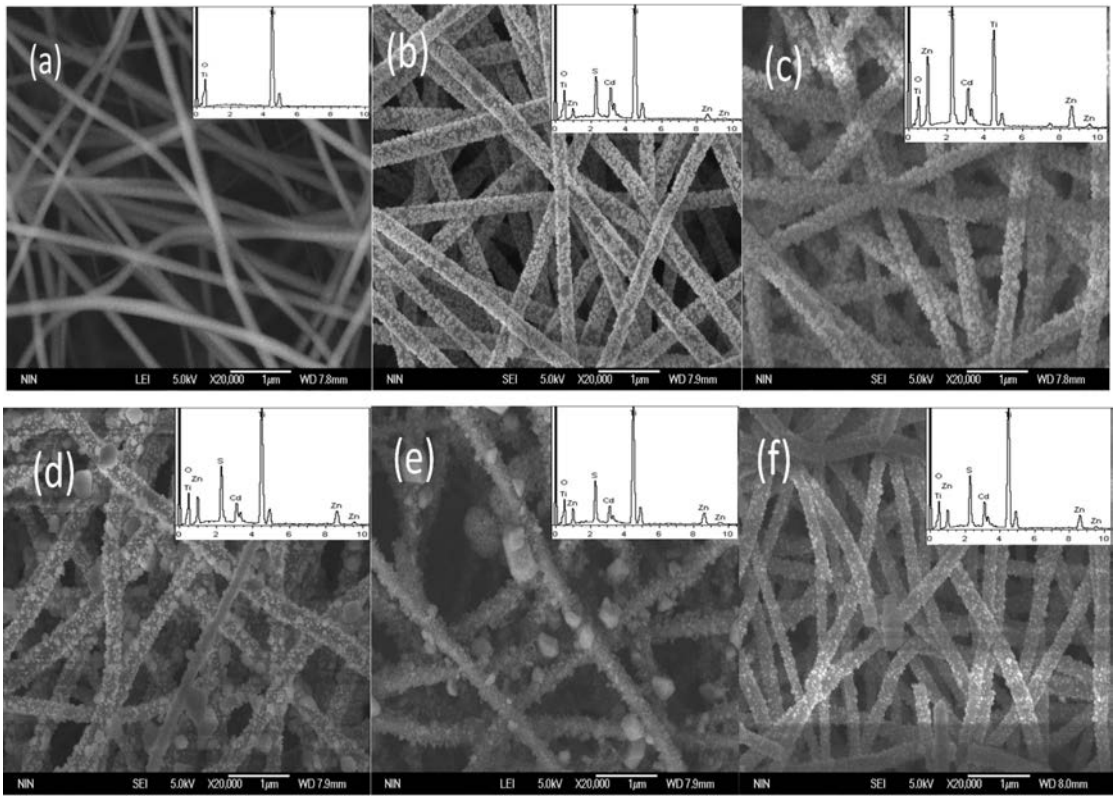

Figure 2 SEM and EDS of sample (**a**) TiO_2 nanofibers, (**b**) S0.5, (**c**) S1, (**d**) S2, (**e**) S3, (**f**) S4.

Cd^{2+} in the solution system decreased, eventually reducing the adhesion amount of $Zn_xCd_{1-x}S$ nanoparticles on the TiO_2 nanofibres.

Meanwhile, the components of each of the prepared samples were studies with X-ray energy dispersive spectroscopy (EDS). As shown in Fig. 2, pure TiO_2 nanofibres are only composed of two elements which are Ti and O. The other five samples are composed of five elements which are Ti, O, Cd, Zn and S. There is no other impurity element observed.

3.3. UV-vis Diffuse Reflectance Spectra

Figure 3 shows UV-vis diffuse reflectance spectra of the as-prepared TiO_2 nanofibres and Zn_xCd_{1-x}/TiO_2 hierarchical heterostructures. The spectrum of the pure TiO_2 nanofibres exhibited the typical absorption behaviour of a wide-band-gap oxide semiconductor, having an intense absorption band with a steep edge at about 400 nm. S0.5, S1, S2, S3 and S4 had new absorption bands between 500 nm and 600 nm. This indicated that the spectral response range of the TiO_2 compos-

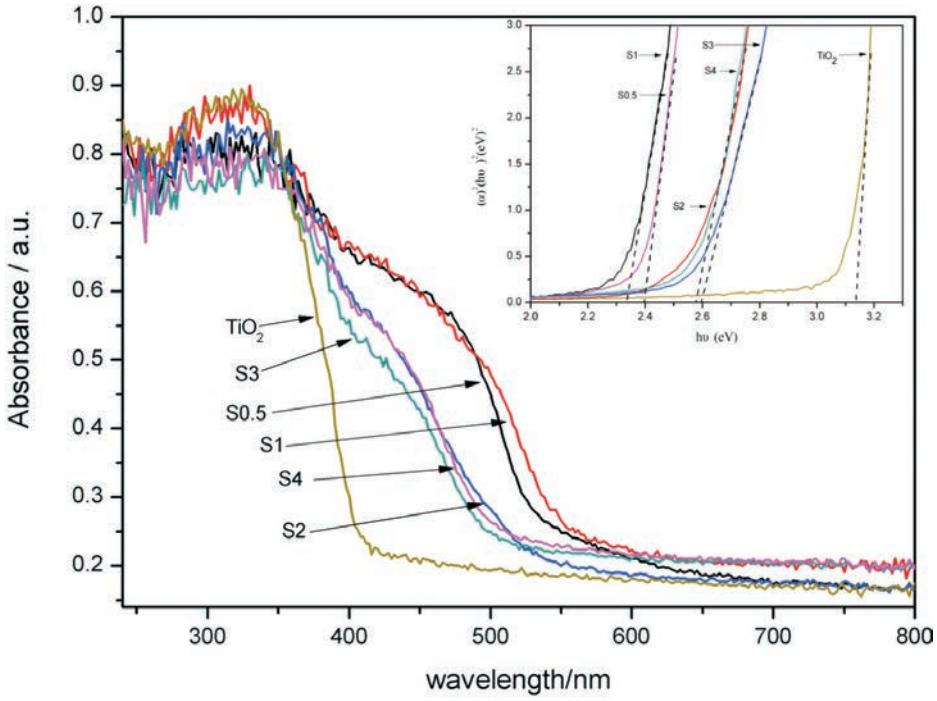

Figure 3 UV-vis diffuse reflectance spectra of TiO_2, S0.5, S1, S2, S3, S4.

ite extended to the visible region due to the $Zn_xCd_{1-x}S$ nanoparticles. For the $Zn_xCd_{1-x}S/TiO_2$ heterostructures, the absorption edge of sample S1 was about 530 nm. Compared with S1, the absorption edge of samples S0.5, S2, S3 and S4 all showed a significant blue-shift. For a crystalline semiconductor, the band gap energy can be calculated by the Kubelka-Munk equation:[19]

$$\alpha h\upsilon = K(h\upsilon - Eg)^2 \quad (1)$$

where $\alpha = (1 - R)^2/2R$, $R = 10^{-A}$, A is an optical absorption, h is Planck constant, υ is photon frequency, K is constant. The results are shown in Table 1. The band gap energy of the pure TiO_2 was about 3.14 eV and the band gap of $Zn_xCd_{1-x}S/TiO_2$ heterostructures ranges from 2.33–2.60 eV. S1 has a minimum band gap energy of 2.33 eV.

3.4 Photocatalytic Activity

The temporal spectral changes of aqueous RhB solutions under visible light irradiation in the presence of the as-prepared samples are presented in Fig. 4. As expected, with 60 min irradiation, all the samples of $Zn_xCd_{1-x}S/TiO_2$ heterostructures showed an improved photocatalytic activity in comparison to the pure TiO_2 nanofibres. This may be attributed to the cooperative roles of $Zn_xCd_{1-x}S$ loading on TiO_2, i.e. a photosensitizing effect of $Zn_xCd_{1-x}S$. $Zn_xCd_{1-x}S$ has a narrow band gap energy. This can be easily excited by visible light to induce the generation of photoelectrons and holes. In the case of TiO_2 nanofibre, it could not be excited by visible light irradiation with energy less than 2.95 eV due to its wide band gap energy of about 3.14 eV, as observed in this work. When $Zn_xCd_{1-x}S/TiO_2$ heterostructures were used as the photocatalysts, $Zn_xCd_{1-x}S$ appears to act as a sensitizer to absorb the visible light. Under visible light irradition, electrons in the valence band of $Zn_xCd_{1-x}S$ are excited to a higher potential edge. The CB edge potential of $Zn_xCd_{1-x}S$ is more active than that of TiO_2, in such a way, the photoinduced electron hole pairs are effectively separated. Moreover, the formed junction between $Zn_xCd_{1-x}S$ and TiO_2 in the heterostructured photocatalysts will further prevent the recombination between photoelectrons and holes. These well-separated photoelectrons and holes will further contribute to the degradation of the dye molecules. Meanwhile, the generated conduction band electrons (e^-) of TiO_2 probably reacted with dissolved oxygen molecules to yield superoxide radical anions (O_2^-), with protonation which generated the hydroperoxy radicals (HO_2^-), producing the hydroxyl radical OH, which is known to be a strong oxidizing agent,[20] to decompose the organic dye. Therefore, the $Zn_xCd_{1-x}S/TiO_2$ heterostructures exhibits better photocatalytic properties than that of TiO_2 on the degradation of RhB under visible light irradiation. Besides, it can be seen from Table 1 that S1 has a larger loading of $Zn_xCd_{1-x}S$ and a narrow band gap. The larger loading of $Zn_xCd_{1-x}S$ appears to improve the optical absorption efficiency and the narrow band gap could increase the visible light absorption. Thus it will result in more stimulated electronic transfer to the conduction band and increase the carrier concentration and promote the photocatalytic degradation reaction. Therefore, S1 exhibits the best performance on the photodegradation of RhB among the five prepared samples. These results are presented in Table 1. After visible light irradiation of 60 min, 92.42 % of RhB was degraded with the S1 photocatalyst, which is much higher than other prepared photocatalysts.

The kinetic profiles for the degradation of RhB in aqueous solution under visible light were also investigated. Figure 5 depicts the $\ln(C_0/C)$ of RhB *versus* irradiation time for the different catalysts. The approximate linear relationship of $\ln(C_0/C)$ *versus* time indicates that the photodegradation process of RhB tend to follow Langmuir-Hinshelwood first-order kinetics model in the presence of the as-prepared catalysts. The kinetics can be expressed as follows: $\ln(C_0/C) = kt$, where k is the apparent reaction rate constant, C_0 is the concentration of RhB at adsorption equilibrium, and C is the residual concentration of RhB at different time intervals. The apparent reaction rate constant k of the different catalyst was identified in Fig. 5. The order of rate constants is summarized as follows: S1>S2>S3>S4>S0.5>TiO_2, which coincides well with the conclusion of the photocatalytic degradation curves presented in Fig. 4.

Table 1 Energy band, S/Ti and degradation rate of different catalyst.

Photocatalyst	TiO_2	S0.5	S1	S2	S3	S4
Energy band/eV	3.14	2.40	2.33	2.59	2.60	2.59
S/Ti		0.25	0.96	0.38	0.26	0.31
Degradation rate/100 %	26.74	32.69	92.42	52.74	41.83	39.81

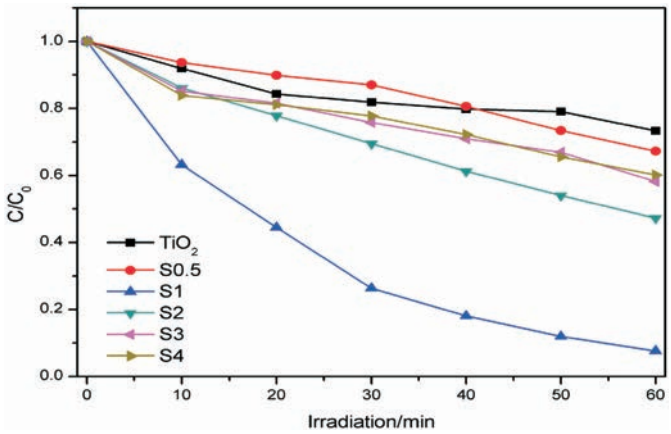

Figure 4 Degradation curve of RhB over different catalysts under visible light.

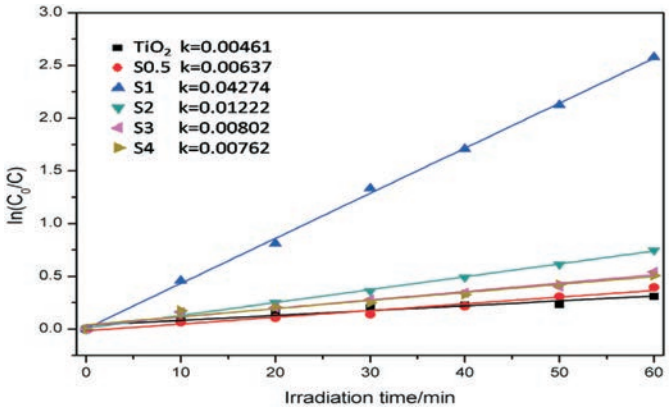

Figure 5 The kinetic curves of degradation of RhB solution under visible light for different catalysts.

4. Conclusions

The $Zn_xCd_{1-x}S/TiO_2$ hierarchical heterostructures with novel architectures were successfully fabricated by using electrospinning technology and hydrothermal processes. The results indicated that the composition and morphology of $Zn_xCd_{1-x}S/TiO_2$ are controlled by changing the sulphur concentration. The fastest photocatalytic decomposition rate of aqueous RhB solution was observed when S/Ti was 0.96, the photocatalytic degradation of RhB followed first-order reaction kinetics and the first-order constant was 0.04274 min^{-1}. Thus the $Zn_xCd_{1-x}S/TiO_2$ visible light system can be regarded as a promising candidate for the photodegradation of dyes from wastewaters.

Acknowledgements

This work was supported by the Fundamental Research Funds for the Central Universities of China under Grant 2011JDGZ15 and by the Research and Development Program of Beilin Distric, Xi'an under Grant JX1419.

References

1 S. Leong, A. Razmjou, K. Wang, K. Hapgood and X. Zhang, TiO_2 based photocatalytic membranes: a review, *J. Membr. Sci.*, 2014, **472**, 167–184.

2 C.M. Teh and A.R. Mohamed, Roles of titanium dioxide and ion-doped titanium dioxide on photocatalytic degradation of organic pollutants in aqueous solutions: a review, *J. Alloy. Compd.*, 2011, **509**, 1648–1660.

3 S.D. Delekara, H.M. Yadava, S.N. Acharyb, S.S. Meenac and S.H. Paward, Structural refinement and photocatalytic activity of Fe-doped anatase TiO_2 nanoparticles, *Appl. Surf. Sci.*, 2012, **263**, 536–545.

4 Y.J. Li, T.P. Cao, C.L. Shao and C.H. Wang, Preparation and energy stored photocatalytic properties of WO_3/TiO_2 composite fibers, *Chem. J. Chinese U.*, 2012, **33** ,1552–1558.

5 P. Periyat, S.C. Pillai, D.E. McCormack, J. Colreavy and S.J. Hinder, Improved high-temperature stability and sun-light-driven photocatalytic activity of sulfur-doped anatase TiO_2, *J. Phys. Chem. C*, 2008, **112**, 7644–7652.

6 X. Li, P. Liu, Y. Mao, M. Xing and J. Zhang, Preparation of homogeneous nitrogen-doped mesoporous TiO_2 spheres with enhanced visible-light photocatalysis, *Appl. Catal. B – Environ.*, 2015, **164**, 352–359.

7 T.Y. Peng, K. Dai and H.B. Yi, Photosensitization of different ruthenium(II) complex dyes on TiO_2 for photocatalytic H_2 evolution under visible-light, *Chem. Phys. Lett.*, 2008, **460**, 216–219.

8 M.Y. Zhang, C.L. Shao and Z.C. Guo, Hierarchical nanostructures of copper(II) phthalocyanine on electrospun TiO_2 nanofibers: controllable solvothermal-fabrication and enhanced visible photocatalytic properties, *ACS App. Mater. Inter.*, 2011, **3**, 369–377.

9 Y. Huo, X. Yang and J. Zhu, Highly active and stable CdS-TiO_2 Visible photocatalyst prepared by *in situ* sulfurization under supercritical conditions, *Appl. Catal. B-Environ.*, 2011, **106**, 69–75.

10 G.F. Ortiz, I. Hanzu and P.Lavela, Nanoarchitectured TiO_2/SnO_2: a future negative electrode for high power density Li-ion microbatteries, *Chem. Mater.*, 2010, **22**, 1926–1932.

11 T. Ju, R.L. Graham and G. Zhai, High Efficiency mesoporous titanium oxide PbS quantum dot solar cells at low temperature, *Appl. Phys. Lett.*, 2010, **97**, 043106-043106-3.

12 X.H. Zhang, D.W. Jing and M.C. Liu, Efficient photocatalytic H_2 production under visible light irradiation over Ni doped $Cd_{1-x}Zn_xS$ microsphere photocatalysts, *Catal. Commun.*, 2008, **9**, 1720–1724.

13 C.H. Zhou and L.J. Guo, $Cd_{1-x}Zn_xS$ energy band calculated by the first-principle method, *J. Xian Jiaotong U.* 2008, **42**, 248–251.

14 Y.X. Li, D. Gao and S.Q. Peng, Photocatalytic hydrogen evolution over $Pt/Cd_{0.5}$ $Zn_{0.5}S$ From saltwater using glucose as electron donor: an investigation of the influence of electrolyte NaCl. *Int. J. Hydrogen Energ.*, 2011, **36**, 4291–4297.

15 G.Liu, Z.Zhou and L.guo, Correlation Between Band Structures and Photocatalytic Activities of $Cd_xCu_yZn_{1-x-y}S$ Solid Solution, *Chem. Phys. Lett.*, 2011, **509**, 43–47.

16 Z. Zhang, C. Shao, X. Li, Y. Sun, M. Zhang, J. Mu, P. Zhang, Z. Guo, and Y. Liu, Hierarchical assembly of ultrathin hexagonal SnS_2 nanosheets onto electrospun TiO_2 nanofibers: enhanced photocatalytic activity based on photoinduced interfacial charge transfer, *Nanoscale*, 2013, **5**, 606–618.

17 S. Ramakrishna, K. Fujihara, W.E. Teo, T. Yong, Z. Ma and R. Ramaseshan, Electrospun nanofibers: solving global issues, *Mater. Today*, 2006, **9**, 40–50.

18 C.H. Wang, C.L. Shao and Y.C. Liu, SnO_2 Nanostructures-TiO_2 nanofibers heterostructrues: controlled fabrication and high photocatalytic properties, *J. Inorg. Chem.*, 2009, **48**, 1105–1113.

19 M. Zhang, C. Shao, J. Mu, Z. Zhang, Z. Guo, P. Zhang and Y. Liu, One-dimensional Bi_2MoO_6/TiO_2 hierarchical heterostructures with enhanced photocatalytic activity, *Cryst. Eng. Comm.*, 2012, **14**, 605–612.

20 J.Zhang, J.H. Bang and C.C.Tang, Tailored TiO_2-$SrTiO_3$ Heterostructure nanotube arrays for improved photoelectrochemical performance, *ACS Nano.*, 2010, **4**, 387–395.